1-1-2012

Combustion Synthesis of Fe-Incorporated SnO2 Nanoparticles Using Organometallic Precursor Combination

Thomas Barkley

Jenna Vastano

James Applegate

Smitesh Bakrania
Rowan University

Recommended Citation

Barkley, T.K., Vastano, J.E., Applegate, J.R., and Bakrania, S.D. (2012). Combustion synthesis of Fe-incorporated SnO2 nanoparticles using organometallic precursor combination. Advances in Materials Science and Engineering, 2012, 685754.

Research Article

Combustion Synthesis of Fe-Incorporated SnO$_2$ Nanoparticles Using Organometallic Precursor Combination

Thomas K. Barkley, Jenna E. Vastano, James R. Applegate, and Smitesh D. Bakrania

Department of Mechanical Engineering, Rowan University, 201 Mullica Hill Road, Glassboro, NJ 08028, USA

Correspondence should be addressed to Smitesh D. Bakrania, bakrania@rowan.edu

Synthesis of nanomaterials within flames has been demonstrated as a highly scalable and versatile approach for obtaining a variety of nanoparticles with respect to their chemistry, composition, size, morphology, and dimensionality. Its applicability can be amplified by exploring new material systems and providing further control over the particle characteristics. This study focused on iron-incorporated SnO$_2$ nanoparticles generated using an inverse coflow diffusion flame burner that supported a near-stoichiometric methane-air combustion. A liquid organometallic precursor solution of Sn(CH$_3$)$_4$ and Fe(CO)$_5$ was used to produce 11–14 nm nanocrystalline particles. Synthesized particles were analyzed using TEM, XRD, and XEDS to characterize for size and composition. A flame temperature field was obtained to map particle evolution within the flame. A range of conditions and parameters were studied to specifically generate targeted particles. The study augments related research towards increasing the production potential of combustion synthesis.

1. Introduction

Nanoparticles are becoming increasingly valuable for applications in a wide range of engineering systems. In addition to uses in many electrical and catalytic applications, nanoparticles such as tin dioxide (SnO$_2$) show great potential as sensing agents in solid-state gas detectors [1, 2]. High aspect ratio SnO$_2$ particles have been demonstrated to improve sensitivity and selectivity of toxic gas detectors [3, 4]. Performance of these particles is highly dependent on morphology, composition, and size [5–9]. For instance, iron-doped SnO$_2$ nanoparticles have been shown as strong candidates for potent gas sensing materials with improved selectivity towards methane, butane, and H$_2$S [10, 11]. At the same time, these nanoparticles are being actively researched for their diluted magnetic semiconductor (DMS) properties [12–14]. Current efforts are focused on the research of effective production methods for such nanomaterials—production methods that are facile and robust for scaleup.

Various chemical and physical synthesis methods have been employed to generate composite or iron-doped SnO$_2$ materials, including coprecipitation [10, 14], mechanical alloying [12], cosputtering [1, 6], sol-gel method [13], and others [11, 15]. However, the need for vacuum conditions or solvents is a considerable hurdle for potential scaleup. Combustions synthesis, on the other hand, offers many advantages over these methods [16–21]. The process is self-purifying, continuous, and affords appreciably high production rates. Current commercial production rates approach several million metric tons/year [16, 17, 22]. Additionally, one-dimensional iron-doped SnO$_2$ structures [23] and thin films [2] have already been successfully produced using combustion synthesis approaches. These approaches, however, use chloride-based precursors that can potentially poison the product materials depending on the application [24, 25] or require absorption of the hydrochloric acid as a byproduct [23]. Though SnO$_2$ and F$_2$O$_3$ nanoparticles have been generated from organometallic precursors individually, a combined combustion synthesis from these precursors has yet to be investigated. As a result, there is a need to explore other compatible precursors for synthesis of iron-doped SnO$_2$ nanoparticles, specifically structures other than commonly found composite nanoarchitectures.

This paper describes a new method to produce iron-incorporated SnO_2 which uses a combination of organometallic precursors in a one-step solvent-free combustion synthesis technique. A bench-top coflow diffusion flame burner was designed for combustion synthesis and sampling of nanoparticles. The facility was configured to deliver a premixed iron pentacarbonyl (IPC) and tetramethyl tin (TMT) precursor solution to an inverse diffusion flame. Based on the particle size, morphology, and chemical composition of the product powders, a model of particle formation is suggested that relies on the effects of flame environment on precursor decomposition and the unique compositional features of the nanoparticles. Therefore, the current work adds to the vast library of nanomaterials that are feasible via combustion synthesis.

2. Experimental Procedure

The facility was designed to provide a compact experimental apparatus with a highly configurable flame environment. The facility exhibited concentric steel tubes to support a flame with four chambers corresponding to the flow of fuel, oxidizer, precursor carrier gas, and the exterior shroud gas. The combustion-synthesized particles were collected on a water-cooled bulk sampling plate. Transmission Electron Microscope (TEM) sampling was performed via pneumatic piston-cylinder actuator. For these experiments, the nanopowders were synthesized using a methane-air inverse diffusion flame. Argon was used as a carrier gas to deliver the liquid-phase precursor solution to the high-temperature reaction zone.

2.1. Experimental Facility. Figure 1 presents a schematic of the custom-built facility for combustion synthesis. The inner diameter of the tube supplying the fuel was 7.6 mm, while the inner diameter of the precursor delivery tube at the burner exit was 1.7 mm. Omega FLD Series rotameters were used to monitor flow rates of the reaction gases. Methane (CH_4, 99.99%, Praxair) flow rate was maintained at 180 mL/min and argon carrier gas (Ar, 99.998%, GTS-Welco) flow rate at 50 mL/min. Depending on the precursor selection, compressed air (99.8%, GTS-Welco) flow rates ranged from 1800 to 2300 mL/min. Gases were configured to yield an inverse diffusion flame at the co-flow burner exit. No shroud gas was used for these experiments. A steel tube chimney with dimensions 108 mm diameter and 254 mm height was used to improve collection efficiency of the products. The precursor reservoir with 21 mL capacity and 6.35 mm diameter glass beads was used to deliver vapor-phase precursors simultaneously to the synthesis region by bubbling argon through the precursor solution.

The synthesis products were collected in two ways. TEM samples were collected using a compressed air piston-cylinder actuator with a mounted 3 mm grid (300 mesh copper grid with carbon film). Typical residence time for the collection in the flame was 2 ms, measured using a high-speed imaging camera. Bulk samples were thermophoretically collected on microscope glass slides mounted on an aluminum block that was maintained at a nominal temperature of 22°C.
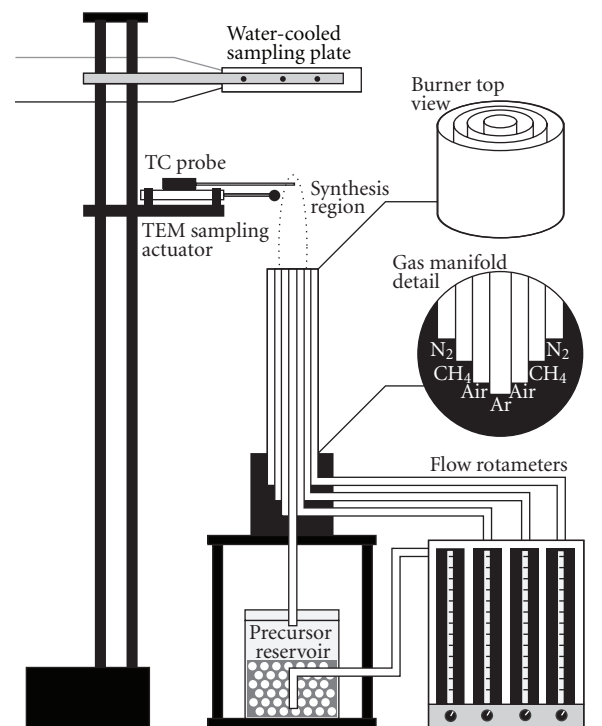

FIGURE 1: A custom-built bench-top coflow diffusion burner with premixed precursor delivery bubbler unit. Piston-cylinder actuator for TEM sampling and water-cooled bulk sampling plate for nanopowder collection.

The bulk sampling plate was typically located at 120 mm above the surface of the burner with a maximum collection time of 10 mins. The flame region was characterized for average temperature at multiple locations along the vertical axis of the burner using S-type thermocouple with a bead diameter of 10 μm. The thermocouple was threaded through an alumina sheathing for temperature measurements, and the temperature readings were corrected to account for radiative heat loss.

2.2. Chemistry. Synthesis of nanopowders was carried out by combusting a solution of liquid-phase iron pentacarbonyl (IPC, $Fe(CO)_5$, >99.99% trace metals basis, Sigma Aldrich) and tetramethyl tin (TMT, $Sn(CH_3)_4$, 95% purity, Sigma Aldrich) precursors. Table 1 lists the relevant thermophysical properties of these chemicals as obtained from the supplier. Of interest are the boiling points, flash points, and phase of the precursors. These properties were comparable for the precursors considering the steep temperature gradients in the flame which ensured the compatibility of these precursors for the current premixed delivery system. In the delivery system, the solution was contained in a bubbler reservoir, where glass beads were included to facilitate evaporation of the liquid mixture. Argon gas was bubbled through the reservoir at room temperature. Low boiling points of the precursors yielded nearly saturated argon gas flow. An entrained precursor solution of 2.5 at % IPC in TMT was targeted for delivery to the burner exit.

TABLE 1: Relevant thermophysical properties of tetramethyl tin (TMT) and iron pentacarbonyl (IPC) with respect to the combustion synthesis environment.

Property	$Sn(CH_3)_4$	$Fe(CO)_5$
Melting point	−54°C	−20°C
Boiling point	75°C	103°C
Flash point	−12°C	−15°C
Phase	Liquid	Liquid

Using global reactions for the stoichiometric combustion of CH_4, TMT, and IPC fuels, experiments were conducted to yield near-stoichiometric combustion of all the fuels (or precursors). Therefore, the air flow rate was adjusted for complete oxidation of precursors while keeping the CH_4 flow rate constant.

2.3. Material Characterization. The solid-phase combustion products were characterized for size, morphology, and chemical composition using a variety of methods. Scanning electron microscopy (SEM, LEO 1530) was used for bulk material morphology, while TEM imaging (Hitachi H-600AB) was performed for detailed size and morphology analysis. Particle size distributions were obtained using a semiautomated MATLAB-based approach described in Bakrania et al. [26] for particle counts exceeding 100. X-ray diffraction (XRD) analysis on the powders was performed using Scintag LT-801 with Cu-Kα X-ray source. Average crystallite size was estimated using Scherrer crystallite size analysis. X-ray energy dispersive spectroscopy (XEDS) was performed on samples in conjunction with the SEM imaging, while inductively coupled plasma (ICP) analysis was performed to study the elemental composition of the products.

3. Results

3.1. Combustion Environment. The co-flow methane-air inverse diffusion flame at the specified flow rates resulted in a blue flame approximately 65 mm in height without the precursor solution present. As the precursor solution was introduced through the central precursor tube, a yellow luminous flame resulted indicating particle formation (see Figure 2). To ensure both precursors were delivered to the flame region, individual precursors (pure TMT and pure IPC) were tested separately. The pure precursors yielded the distinct luminous flames to produce respective iron oxide and tin dioxide as demonstrated by several other studies [21, 22, 26–31]. To introduce catalytic quantities of iron in the product powders, 2.5 at% IPC was added to TMT in the bubbler and sealed. The introduction of this precursor solution produced a distinctly luminous flame compared to the pure TMT system.

Flame temperatures were measured along the height of the flame at the central axis to characterize the reaction zone using a thermocouple mounted to the sampling stand. Temperatures were measured for three different systems for comparison: methane-air flame without precursor solution, pure TMT as the precursor, and a solution of 2.5 at% IPC in TMT. Figure 3 presents the temperature profile with
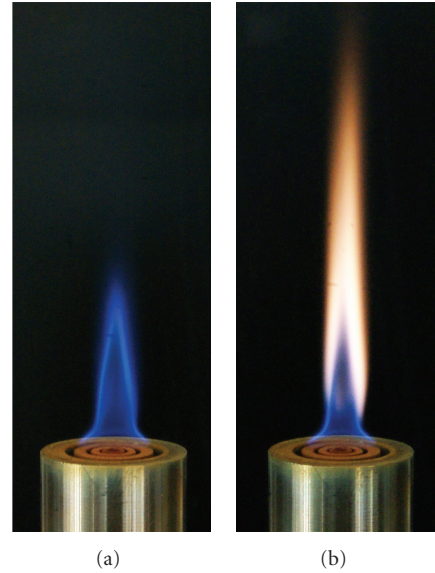

(a) (b)

FIGURE 2: Images of the inverted diffusion flame (a) without precursors and (b) with a mixture of 2.5 at% IPC in TMT present. As a reference, the external diameter of the burner is 20.3 mm.

a rapid increase in temperature from just above the burner surface to a gradual drop in temperature at higher locations for all three systems. The peak temperature was observed at approximately 23 mm above the burner for all three systems. The flame without any precursor exhibited a peak temperature of ~1100°C, while the flame with pure TMT observed a drop in peak temperature to ~900°C that can be attributed to the cooling from the additional vapor-phase precursor solution. The high peak temperature of ~1300°C for the IPC-TMT system can be explained by the highly exothermic decomposition of precursors which, as a result, yields relatively higher temperatures in the product gases as well. The temperatures were corrected for radiation, and the relative uncertainty for the measured temperatures was estimated at 5%. Any inadvertent material deposits on the thermocouple were cleared for accurate assessment of flame temperatures.

3.2. Material Characterization. The combustion-synthesized powders were collected on microscope slides at a rate of 3–5 mg/min. Grayish-white fine powders were obtained with the IPC-TMT precursor solution at a height of 117 mm on the water-cooled sampling plate. The tubular steel chimney was only used for XRD sampling runs. Figure 4 presents an XRD spectra of the 2.5 at% IPC-TMT precursor solution product as obtained from the experiments. All the peaks were identified for the cassiterite phase of SnO_2 (JCPDS Ref. No. 41–1445), while no peaks were attributed to any iron or iron-based compounds. Scherrer crystallite size analysis performed on the 110 peak of SnO_2 yielded average crystallite size of 16.4 nm for the SnO_2 particles.

Figures 5(a) and 5(b) provide SEM images of the bulk samples demonstrating granular structure at lower magnification while a porous architecture is identified for the individual grains, respectively. XEDS analysis conducted on the
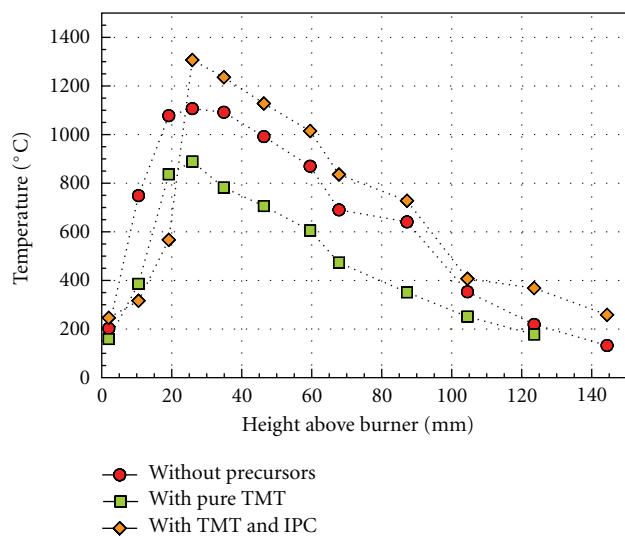
FIGURE 3: Radiation-corrected thermocouple temperature measurements above the central axis of the burner. Plot includes temperature profiles for the reaction zone without precursors, with pure TMT, and with 2.5 at% IPC-TMT precursor solution.
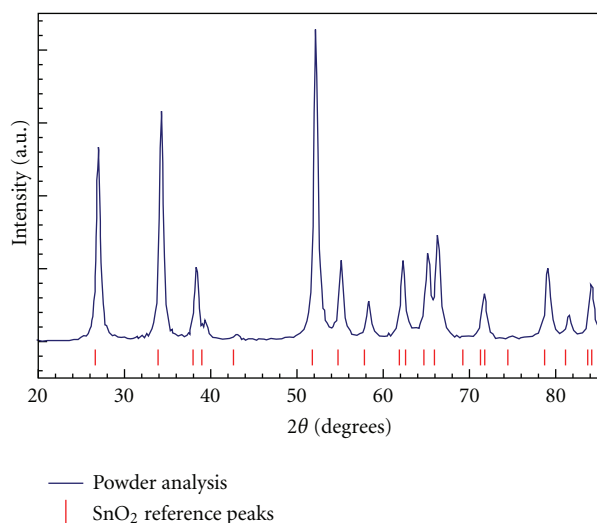

FIGURE 4: X-ray diffraction spectra of 2.5 at% IPC-TMT precursor solution products. Peaks identified as cassiterite phase SnO_2. No peaks were attributed to the presence of any iron or iron-based compounds.

SEM samples confirmed the presence of tin (Sn) and oxygen (O), at the same time indicating presence of elemental iron (Fe) at 3.3 wt% (6.8 at%). The presence of elemental iron was also confirmed using inductively couple plasma (ICP) analysis yielding atomic ratio of 0.069 for Fe : Sn (2.2 at% Fe in SnO_2 assuming stoichiometric oxygen content for tin), which corroborates well with initial precursor concentration. Figures 5(c) and 5(d) are TEM images of grid samples collected using the actuated piston cylinder at a height of 46 mm. These samples show typically spherical primary nanoparticles forming agglomerated nanostructures.

TEM images were used to determine the particle size distribution of the primary particles using a semiautomated image analysis. Figure 6 provides a primary particle size distribution obtained for multiple TEM images originating from a single sampling at 64 mm height above the burner. As seen, the geometric mean of 11.4 nm was calculated for the precursor solution samples with over 150 particles counted. A subsequent study on how the average primary particle size varies above the height of the burner at three locations (25 mm, 33 mm, and 41 mm) yielded average primary particle sizes of 6.8 nm, 8.7 nm, and 14.3 nm above the burner surface, respectively, demonstrating an appreciable growth as the particles move across the peak flame temperatures at ~23 mm above the burner surface. The calculated average primary particle sizes (11–14 nm) correspond well with the XRD crystallite sizes analyzed (16 nm) using Scherrer analysis considering differences in the two approaches— suggesting majority of the primary particles exist as single crystals.

3.3. Investigating Iron. Considering no iron compounds were identified using XRD other than the elemental presence detected using ICP and XEDS, two possibilities exist for the ultimate fate of Fe presence in SnO_2 nanoparticles: (a) the iron compounds (most probably oxides) are at low enough concentrations in the products that they cannot be distinctly identified with XRD or (b) the iron is incorporated into the SnO_2 lattice, generating iron-doped tin dioxide nanopowders. To investigate the first hypothesis, an increased concentration of 10 at% IPC in TMT was tested to produce a higher iron-based component within tin dioxide nanopowders to assist XRD identification. Subsequent XRD analyses of the products from 10 at% IPC yielded identical results when compared to the 2.5 at% IPC—only cassiterite-phase tin dioxide was identified while no peaks could be attributed to any iron or iron based compound. These results are in agreement with the recently published work by Alexandrescu and co-workers [32] using IPC and TMT as precursors with laser pyrolysis, where no iron compounds were identified. Melghit and Bouziane [15] also demonstrated the absence of iron-based compounds in tin dioxide powders and attributed the outcome to Fe atoms substituting Sn in the lattice with comparable iron concentrations to this study. Additionally, the nanopowders with higher iron-content, when analyzed with TEM image analysis, produced a mean primary particle size of 13 nm with over 500 particles counted (sampled at 64 mm height). XRD analysis yielded crystallite diameter of 14.5 nm for these samples. Therefore, no appreciable change in primary particle size was observed with increased IPC concentration.

4. Discussion

The literature presents several examples of precursor's properties and chemistry influencing the resulting product materials in combustion synthesis [33–36]. Therefore, the choice of specific precursors used in this study was deliberate to ensure doped products as opposed to nanocomposites metal oxides. Figure 7 presents a schematic of how a relatively
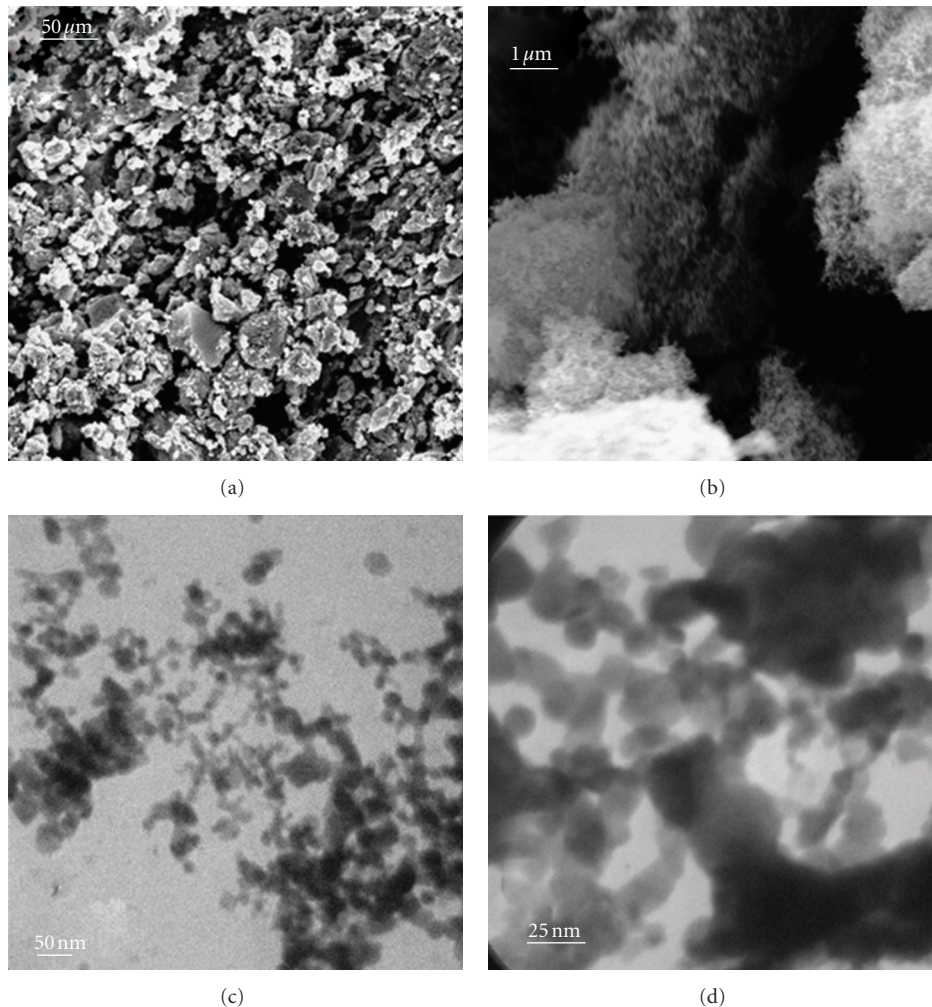
(a)

(b)

(c)

(d)

FIGURE 5: SEM and TEM images of nanoparticle products from the combustion synthesis. The majority of the powders were identified as tin dioxide using XEDS analysis.

large difference in decomposition temperatures of component precursors in a solution can yield different nanoparticle architectures: composites versus doped or solid-solution systems. When the decomposition temperatures are significantly different (or involve varying phase precursors), the subsequent particle formation is decoupled between the two component systems leading to a composite system (left on Figure 7), while a relatively similar decomposition temperature and particle formation time scales can potentially lead to a doped or a solid solution system (right on Figure 7). A doped system also has to be favored by the atomic or ionic radii interactions within the specific crystal structure [1, 11]. On the other hand, higher doping levels can result in phase segregation within a solid-solution to ultimately yield a nanocomposite system that is commonly observed in alloying [37]. For the current system, it can be assumed the later scenarios dominate for the Fe-incorporated SnO_2 material obtained. Vapor-phase TMT decomposition can occur at much lower temperatures than documented decomposition temperatures [38] and IPC already exhibits decomposition temperature that is as low as 200°C. Therefore, early com-

parable decomposition locations for the two precursors and subsequent particle formation steps can be attributed to the observed particle composition.

More importantly, the absence of iron-based compounds from XRD analysis can be sufficiently explained by a conclusive investigation conducted by Castro and coworkers [39] on SnO_2-Fe_2O_3 nanopowders. Their work demonstrated and confirmed surface segregation of iron phases as the concentration of iron increased within SnO_2. As a result of this phenomenon, at lower concentrations of up to 30 mol % Fe, no identifiable features of iron-based compounds are present on X-ray spectra of SnO_2. The eventual encapsulation of SnO_2 was supported by the combination of XEDS and HRTEM analysis on the particles as a function of Fe concentration. The work by Castro et al. substantiates the observations on combustion-synthesized powders presented here and results of other similar studies [15, 32].

The primary particle sizes for the combustion-synthesized Fe-incorporated SnO_2 were competitive to nanoparticles obtained using other methods [2, 10, 11, 13]. With respect to the varying concentration of IPC in TMT,

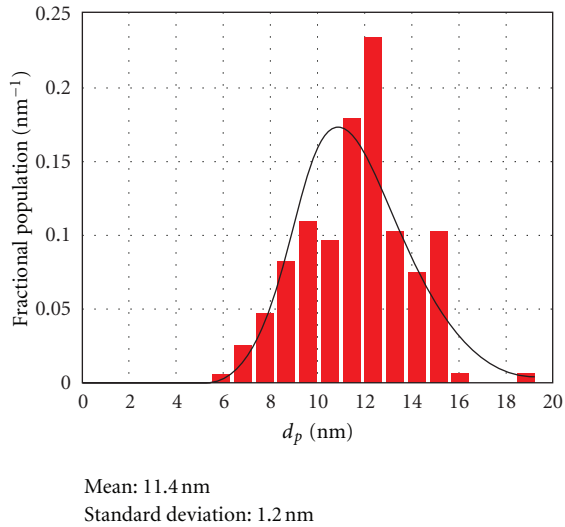chemical sensors," *Progress in Materials Science*, vol. 54, no. 1, pp. 1–67, 2009.

[7] P. M. Rao and X. Zheng, "Flame synthesis of tungsten oxide nanostructures on diverse substrates," *Proceedings of the Combustion Institute*, vol. 33, no. 2, pp. 1891–1898, 2011.

[8] J. Liu, Y. Hu, F. Gu, J. Ma, and C. Li, "Tin oxide nanowires synthesized via flat flame deposition : structures and formation mechanism," *Industrial & Engineering Chemistry Research*, vol. 50, pp. 5584–5588, 2011.

[9] E. R. Leite, I. T. Weber, E. Longo, and J. A. Varela, "New method to control particle size and particle size distribution of SnO$_2$ nanoparticles for gas sensor applications," *Advanced Materials*, vol. 12, no. 13, pp. 965–968, 2000.

[10] S. Chakraborty, A. Sen, and H. S. Maiti, "Selective detection of methane and butane by temperature modulation in iron doped tin oxide sensors," *Sensors and Actuators B*, vol. 115, no. 2, pp. 610–613, 2006.

[11] M. V. Vaishampayan, R. G. Deshmukh, P. Walke, and I. S. Mulla, "Fe-doped SnO$_2$ nanomaterial: a low temperature hydrogen sulfide gas sensor," *Materials Chemistry and Physics*, vol. 109, no. 2-3, pp. 230–234, 2008.

[12] V. Bilovol, A. M. Mudarra Navarro, C. E. Rodríguez Torres, F. H. Sánchez, and A. F. Cabrera, "Magnetic and structural study of Fe doped tin dioxide," *Physica B*, vol. 404, no. 18, pp. 2834–2837, 2009.

[13] S. Sambasivam, B. C. Choi, and J. G. Lin, "Intrinsic magnetism in Fe doped SnO$_2$ nanoparticles," *Journal of Solid State Chemistry*, vol. 184, no. 1, pp. 199–203, 2011.

[14] A. Sharma, M. Varshney, S. Kumar, and R. Kumar, "Magnetic properties of Fe and Ni doped SnO$_2$ nanoparticles," *Nanomaterials and Nanotechnology*, vol. 1, pp. 24–28, 2011.

[15] K. Melghit and K. Bouziane, "One step aqueous solution preparation of nanosize iron-doped tin oxide from SnO$_2$xH$_2$O gel," *Materials Science and Engineering B*, vol. 128, no. 1–3, pp. 58–62, 2006.

[16] M. S. Wooldridge, "Gas-phase combustion synthesis of particles," *Progress in Energy and Combustion Science*, vol. 24, no. 1, pp. 63–87, 1998.

[17] H. K. Kammler, L. Mädler, and S. E. Pratsinis, "Flame synthesis of nanoparticles," *Chemical Engineering and Technology*, vol. 24, no. 6, pp. 583–596, 2001.

[18] H. Takehara, M. Fujiwara, M. Arikawa, M. D. Diener, and J. M. Alford, "Experimental study of industrial scale fullerene production by combustion synthesis," *Carbon*, vol. 43, no. 2, pp. 311–319, 2005.

[19] D. E. Rosner, "Flame synthesis of valuable nanoparticles: recent progress/current needs in areas of rate laws, population dynamics, and characterization," *Industrial and Engineering Chemistry Research*, vol. 44, no. 16, pp. 6045–6055, 2005.

[20] A. I. Y. Tok, F. Y. C. Boey, S. W. Du, and B. K. Wong, "Flame spray synthesis of ZrO$_2$ nano-particles using liquid precursors," *Materials Science and Engineering B*, vol. 130, no. 1–3, pp. 114–119, 2006.

[21] P. Roth, "Particle synthesis in flames," in *Proceedings of the 31st International Symposium on Combustion*, pp. 1773–1788, August 2006.

[22] T. A. Miller, S. D. Bakrania, C. Perez, and M. S. Wooldridge, "A new method for direct preparation of tin dioxide nanocomposite materials," *Journal of Materials Research*, vol. 20, no. 11, pp. 2977–2987, 2005.

[23] J. Liu, F. Gu, Y. Hu, and C. Li, "Flame synthesis of tin oxide nanorods: a continuous and scalable approach," *Journal of Physical Chemistry C*, vol. 114, no. 13, pp. 5867–5870, 2010.

[24] N. Sergent, P. Gélin, L. Périer-Camby, H. Praliaud, and G. Thomas, "Preparation and characterisation of high surface area stannic oxides: structural, textural and semiconducting properties," *Sensors and Actuators B*, vol. 84, no. 2-3, pp. 176–188, 2002.

[25] J. Zhang and L. Gao, "Synthesis and characterization of nanocrystalline tin oxide by sol-gel method," *Journal of Solid State Chemistry*, vol. 177, no. 4-5, pp. 1425–1430, 2004.

[26] S. D. Bakrania, T. A. Miller, C. Perez, and M. S. Wooldridge, "Combustion of multiphase reactants for the synthesis of nanocomposite materials," *Combustion and Flame*, vol. 148, no. 1-2, pp. 76–87, 2007.

[27] K. Buyukhatipoglu and A. Morss Clyne, "Controlled flame synthesis of αFe$_2$O$_3$ and Fe$_3$O$_4$ nanoparticles: effect of flame configuration, flame temperature, and additive loading," *Journal of Nanoparticle Research*, vol. 12, pp. 1495–1508, 2009.

[28] C. Janzen, P. Roth, and B. Rellinghaus, "Characteristics of Fe$_2$O$_3$ nanoparticles from doped low-pressure H$_2$/O$_2$/Ar flames," *Journal of Nanoparticle Research*, vol. 1, no. 2, pp. 163–167, 1999.

[29] C. Janzen, J. Knipping, B. Rellinghaus, and P. Roth, "Formation of silica-embedded iron-oxide nanoparticles in low-pressure flames," *Journal of Nanoparticle Research*, vol. 5, no. 5-6, pp. 589–596, 2003.

[30] M. R. Zachariah, M. I. Aquino, R. D. Shull, and E. B. Steel, "Formation of superparamagnetic nanocomposites from vapor phase condensation in a flame," *Nanostructured Materials*, vol. 5, no. 4, pp. 383–392, 1995.

[31] D. Lindackers, C. Janzen, B. Rellinghaus, E. F. Wassermann, and P. Roth, "Synthesis of Al$_2$O$_3$ and SnO$_2$ particles by oxidation of metalorganic precursors in premixed H$_2$/O$_2$/Ar low pressure flames," *Nanostructured Materials*, vol. 10, no. 8, pp. 1247–1270, 1998.

[32] R. Alexandrescu, I. Morjan, F. Dumitrache et al., "Recent developments in the formation and structure of tin-iron oxides by laser pyrolysis," *Applied Surface Science*, vol. 257, pp. 5460–5464, 2011.

[33] H. Briesen, A. Fuhrmann, and S. E. Pratsinis, "The effect of precursor in flame synthesis of SiO$_2$," *Chemical Engineering Science*, vol. 53, no. 24, pp. 4105–4112, 1998.

[34] A. U. Limaye and J. J. Helble, "Effect of precursor and solvent on morphology of zirconia nanoparticles produced by combustion aerosol synthesis," *Journal of the American Ceramic Society*, vol. 86, no. 2, pp. 273–278, 2003.

[35] R. Strobel and S. E. Pratsinis, "Direct synthesis of maghemite, magnetite and wustite nanoparticles by flame spray pyrolysis," *Advanced Powder Technology*, vol. 20, no. 2, pp. 190–194, 2009.

[36] S. D. Bakrania, G. K. Rathore, and M. S. Wooldridge, "An investigation of the thermal decomposition of gold acetate," *Journal of Thermal Analysis and Calorimetry*, vol. 95, pp. 117–122, 2008.

[37] B. N. Wanjala, J. Luo, B. Fang, D. Mott, and C. -J. Zhong, "Gold-platinum nanoparticles: alloying and phase segregation," *Journal of Materials Chemistry*, vol. 21, no. 12, pp. 4012–4020, 2011.

[38] S. D. Bakrania, C. Perez, and M. S. Wooldridge, "Methane-assisted combustion synthesis of nanocomposite tin dioxide materials," in *Proceedings of the 31st International Symposium on Combustion*, pp. 1797–1804, August 2006.

[39] R. H. R. Castro, P. Hidalgo, J. A. H. Coaquira, J. Bettini, D. Zanchet, and D. Gouvêa, "Surface segregation in SnO$_2$-Fe$_2$O$_3$ nanopowders and effects in mössbauer spectroscopy," *European Journal of Inorganic Chemistry*, no. 11, pp. 2134–2138, 2005.

[40] R. K. Selvan, C. O. Augustin, L. J. Berchmans, and R. Saraswathi, "Combustion synthesis of CuFe$_2$O$_4$," *Materials Research Bulletin*, vol. 38, no. 1, pp. 41–54, 2003.

[41] C. Siriwong and S. Phanichphant, "Flame-made single phase Zn_2TiO_4 nanoparticles," *Materials Letters*, vol. 65, no. 12, pp. 2007–2009, 2011.

[42] P. Pawinrat, O. Mekasuwandumrong, and J. Panpranot, "Synthesis of Au-ZnO and Pt-ZnO nanocomposites by one-step flame spray pyrolysis and its application for photocatalytic degradation of dyes," *Catalysis Communications*, vol. 10, no. 10, pp. 1380–1385, 2009.

[43] V. Tiwari, J. Jiang, V. Sethi, and P. Biswas, "One-step synthesis of noble metal-titanium dioxide nanocomposites in a flame aerosol reactor," *Applied Catalysis A*, vol. 345, no. 2, pp. 241–246, 2008.

[44] A. Teleki, N. Bjelobrk, and S. E. Pratsinis, "Flame-made Nb- and Cu-doped TiO_2 sensors for CO and ethanol," *Sensors and Actuators B*, vol. 130, no. 1, pp. 449–457, 2008.

[45] S. Da Dalt, A. S. Takimi, V. C. Sousa, and C. P. Bergmann, "Magnetic and structural characterization of nanostructured $MgFe_2O_4$ synthesized by combustion reaction," *Particulate Science and Technology*, vol. 27, no. 6, pp. 519–527, 2009.